

Supporting Information

Urocanic acid as a novel scaffold for next-gen nature-inspired sunscreens:

II. Time-resolved spectroscopy under solution conditions

Jiayun Fan, Jack M. Woolley, Hans Sanders, Vasilios Stavros* and Wybren Jan Buma*

Contents

1. Experimental procedures	3
1.1 Photostability studies	3
1.2 Transient electronic absorption spectroscopy	3
1.3 Theoretical methods.....	4
2. Synthesis and characterization	6
3. Photostability studies	7
3.1 UV/vis absorption spectroscopy	7
3.2 NMR.....	7
3.3 FT-IR spectroscopy.....	14
3.4 Population ratios used in FT-IR simulations	18
4. Femtosecond transient absorption spectra in acetonitrile	20
5. Calculations of vertical and adiabatic excitation energies	21
6. Electron scavenging studies	24
7. Nanosecond transient absorption spectra in buffer solutions.....	25
8. Supplemental references	27

1. Experimental procedures

Urocanic acid was purchased from Sigma-Aldrich chemicals and used without any purification. The synthesis of methyl urocanate, N₃-methyl methyl urocanate, and N₁-methyl methyl urocanate have been synthesized in-house using synthetic routes described previously¹, while the synthesis of *cis*-urocanic acid and *cis*-methyl urocanate is described below. The spectroscopic grade solvents employed for the photostability experiments (ethanol, dioxane, and acetonitrile) were purchased from Alfa-Aesar and used as received. The acetate (pH 5.6) and phosphate (pH 7.2) buffer solutions were prepared following standard recipes.^{2,3}

1.1. Photostability studies

In these studies, photodegradation was monitored using UV/vis absorption spectroscopy, IR absorption spectroscopy, and ¹H NMR. For the UV/vis monitoring studies, a tunable Nd:YAG-laser system (NT342B, Ekspla) operating at the maximum absorption wavelength of each sample was used, and samples were prepared at a concentration of 5×10⁻⁵ M in a 1 cm quartz cuvette. To avoid multiphoton degradation processes, pulses with a pulse length of 5 ns and a pulse energy of 6 μJ at a repetition rate of 10 Hz were employed to irradiate the sample for a certain amount of time after which a UV/vis absorption spectrum was taken with a Shimadzu UV-2700 UV/vis spectrometer. For the IR monitoring experiments, samples were prepared at a concentration of 20 mM in a BaF₂ cell with a spacer of 250 μm. The same laser system was employed to irradiate the samples for a specific time but with pulse energies of 15 μJ. FT-IR absorption spectra were recorded with a Bruker Vertex 70 spectrometer. ¹H NMR spectra of samples were taken in deuterated methanol with a 400 MHz NMR spectrometer.

1.2. Transient electronic absorption spectroscopy

Samples were prepared in 25 mL ethanol, dioxane or acetonitrile at a concentration of 1 mM, a concentration that was also used for UA in acetate and phosphate buffer solutions. The samples were circulated using a diaphragm pump (SIMDOS, KNF) through a demountable Harrick Scientific flow-through cell equipped with two CaF₂ windows separated by 950 μm polytetrafluoroethylene spacers to ensure that at each pump–probe pulse sequence, a fresh sample was available. The femtosecond (fs) TEAS setup used to study the photodynamics of UA and its derivatives in various solvents has been described in detail previously,^{4,5} In brief, femtosecond 800 nm pulses (12 W, 1 kHz) were generated by a commercially available, Ti-sapphire regenerative amplified laser system (Spectra-Physics, Dual Ascend Pumped Spitfire Ace) seeded by a Mai Tai (Spectra-Physics). The beam is split into four fractions of approximately equal power, each one having a separate recompression grating. One of these beams (3.5 W) was split once more and utilized to

generate the pump and probe beams for the experiments presented here. A 2.5 W fraction seeds an optical parametric amplifier (Topas-Prime with UV extension, Light Conversion) allowing variability in pump wavelengths. The probe pulses are generated by focusing 5% of the remaining 1 W, 800 nm fundamental beam, which is further attenuated and irised, into a vertically translated CaF₂ window, generating a white light continuum (320–720 nm). The relative polarization between pump and probe pulses was held at magic angle (54.7°) to negate dynamic contributions from molecular reorientation. Pump–probe delays ranging from –1 ps to 2.5 ns are achieved by translating a hollow gold retroreflector on a motorized optical delay line in the probe path (Newport M-IMS500CCHA). Changes in optical density were calculated from the measured probe intensities, collected using a fiber-coupled spectrometer (Avantes, AvaSpec-ULS1650F). For most of the experiments, the pump excitation wavelengths were set at the λ_{max} wavelength except for the buffer solutions where experiments at 306 nm were performed as well. Data obtained with this setup are presented in the main manuscript as well as in the Supporting Information without chirp correction.

Nanosecond (ns) transient absorption spectra on samples with a concentration of 5×10^{-5} M were recorded with an in-house assembled setup described previously.⁶ Briefly, the excitation wavelength was generated using a tunable Nd:YAG-laser system (NT342B, Ekspla) operating at a repetition rate of 10 Hz while the probe light running at 20 Hz was generated by a high-stability short arc xenon flash lamp. Using a 50/50 beam splitter, the probe light was split equally into a signal beam and a reference beam and focused on the entrance slit of a spectrograph (SpectraPro-150, Princeton Instruments). The probe beam ($A = 1 \text{ mm}^2$) was passed through the sample cell and orthogonally overlapped with the excitation beam on a $1 \text{ mm} \times 1 \text{ cm}$ area. To correct for fluctuations in the flash lamp spectral intensity, the reference was used to normalize the signal. Both beams were recorded simultaneously using a gated intensified CCD camera (PI-MAX3, Princeton Instruments).

Analysis of the fs and ns transient absorption spectra has been performed using the Glotaran software package⁷ with which the spectra have been globally fitted using a sequential kinetic model.

1.3. Theoretical methods

The possible conformations UA can adopt are displayed in Figure S1. Each conformation is classified according to the protonation site of the imidazole moiety as either N₃H or N₁H, and the τ_{26} (C₁C₂C₆C₇), τ_{67} (C₂C₆C₇C₈), and τ_{78} (C₆C₇C₈O₉) dihedral angles which can be C(*cis*) ($\sim 0^\circ$) or T(*trans*) ($\sim 180^\circ$). Geometry optimization of the structure of relevant conformers of UA and derivatives in their electronic ground state as well as in electronically excited singlet states, followed by calculations of the harmonic force field has been performed using Time Dependent-Density Functional Theory (TD-DFT) at the wB97XD/cc-pVDZ level in combination with the Polarizable Continuum Model (PCM) to take solvent effects into account.^{8,9} For the calculation of the absorption spectrum of the

lowest excited triplet state, geometry optimizations of T_1 were performed at the Unrestricted Density Functional Theory (UDFT) level, followed by the calculation of excited-state energies and oscillator strengths of $T_n \leftarrow T_1$ transitions by TD-DFT calculations. To compare experimentally recorded IR absorption spectra with theoretically predicted spectra, DFT calculations have been performed on the electronic ground state at the B3LYP/6-31++G(d,p)/PCM level.^{10,11} For these calculations the four lowest-energy *trans* and *cis* conformations were considered. Simulated IR absorption spectra before and after UV radiation were constructed by scaling vibrational frequencies with a factor of 0.975^{12,13} and adding the IR spectra of the individual conformers with their calculated Boltzmann weight. All calculations have been performed with the Gaussian16, Rev.C.01 suite of programs.¹⁴

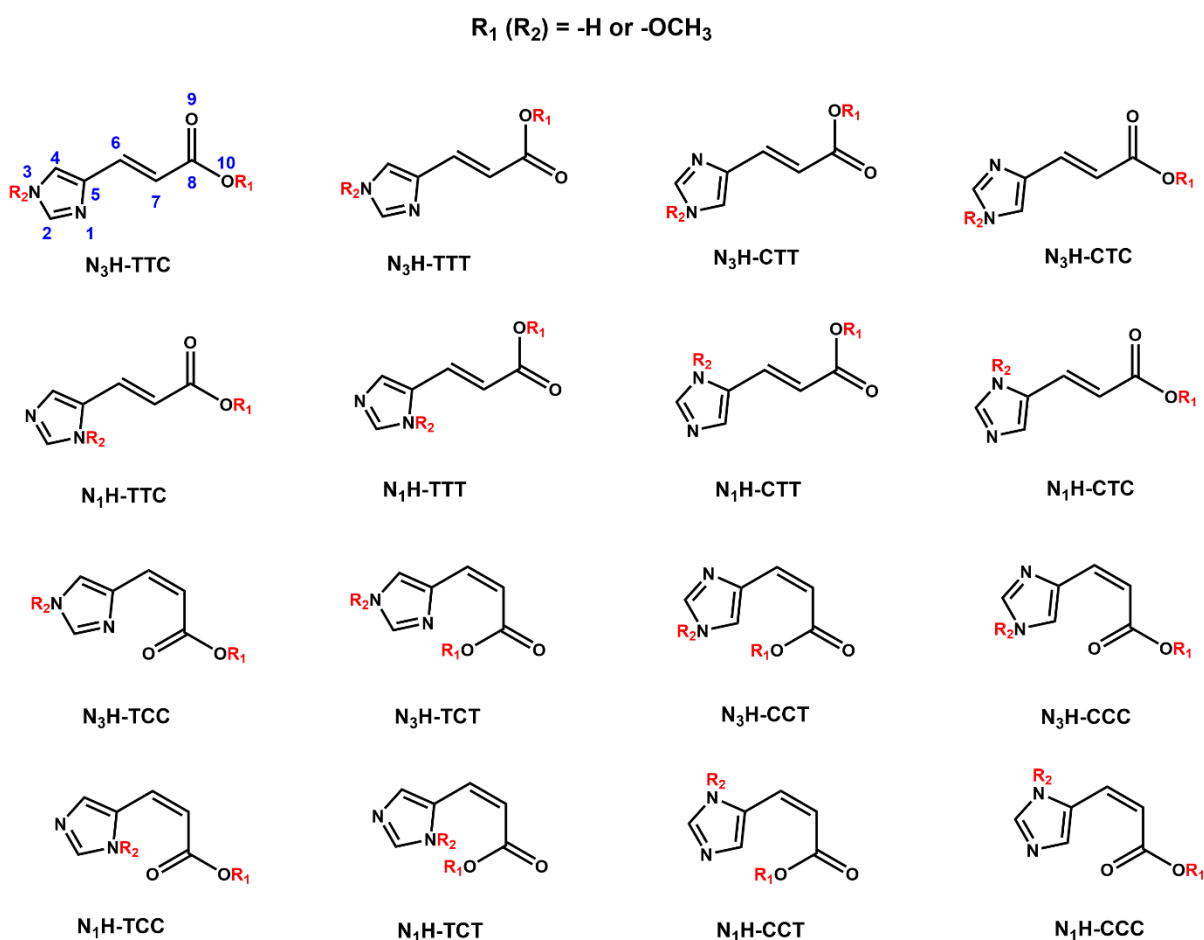


Figure S1. Possible conformations of urocanic acid ($R_1(R_2) = -H$), methyl urocanate ($R_1 = -OCH_3$, $R_2 = -H$), N_3 -(N_1)-methyl methyl urocanate $R_1(R_2) = -OCH_3$.

2. Synthesis and characterization

***Cis*-urocanic acid**

A stirred solution of *trans*-UA (1.5 g, 10.9 mmol) in MeOH (400 mL) in a quartz tube (ϕ 45 mm) was irradiated with 254 nm light from 10 tubular Hg-lamps for 4 h at RT. TLC indicated conversion. The reaction mixture was concentrated in vacuo and the crude product was purified by flash chromatography (SiO₂, gradient elution with CH₂Cl₂/MeOH/25% NH₄OH – 90/10/1 → 85/15/1.5 → 80/20/2 → 70/30/3 → 60/40/4) to afford 0.70 g (yield 47%) of the title product as an off-white solid. ¹H-NMR (DMSO-d₆, 400 MHz) δ 13.07 (vbs, 2H), 8.09 (s, 1H), 7.60 (s, 1H), 6.85 (d, J = 12.8 Hz, 1H), 5.66 (d, J = 12.8 Hz, 1H); TLC R_f \approx 0.3 (SiO₂, 25% CH₂Cl₂/MeOH/25% NH₄OH – 75/25/2.5).

***Cis*-methyl urocanate**

A stirred solution of *trans*-methyl urocanate (0.66 g, 4.34 mmol) in MeOH (200 mL) in a quartz tube (ϕ 45 mm) was irradiated with 254 nm light from 10 tubular Hg-lamps for 2 h at RT. TLC indicated conversion. The reaction mixture was concentrated in vacuo and the crude product was purified by flash chromatography (SiO₂, gradient elution with CH₂Cl₂/MeOH/25% NH₄OH – 99/1/0.1 → 98/2/0.2 → 96/4/0.4 → 92/8/0.8) to afford 0.382 g (yield 58%) of the title product as light brown oil. ¹H-NMR (CDCl₃, 400 MHz) δ 12.77 (bs, 1H), 7.73 (s, 1H), 7.37 (s, 1H), 6.85 (d, J = 12.5 Hz, 1H), 5.69 (d, J = 12.5 Hz, 1H), 3.79 (s, 3H); TLC R_f \approx 0.4 (SiO₂, CH₂Cl₂/MeOH/25% NH₄OH – 95/5/0.5).

3. Photostability studies

3.1. UV/vis absorption spectroscopy

A. Comparison UV/vis spectra irradiated samples in ethanol with spectra of isolated isomers
Figure S2 shows UV/vis spectra of *trans* and *cis* isomers of (a) UA and (b) methyl urocanate in ethanol, and compares these spectra with the UV/vis spectrum obtained upon irradiation of *trans*-UA and *trans*-methyl urocanate. These spectra confirm the blue and red shifts observed in Figure 2(a) and (b) in the main text. They also demonstrate that for UA an almost full *trans*-*cis* conversion is obtained while for methyl urocanate still a mixture of *trans* and *cis* isomers is present under photostationary conditions.

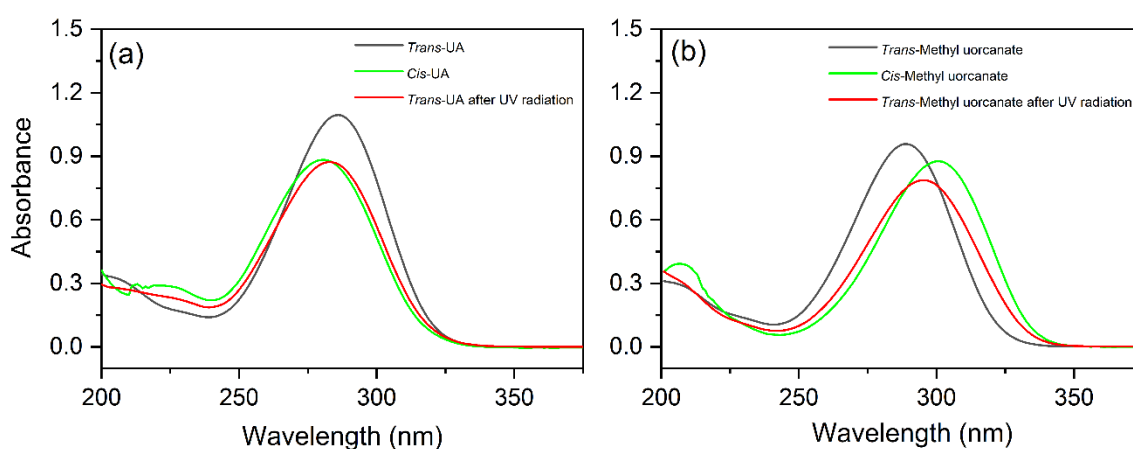


Figure S2. UV/vis spectra of (a) UA and (b) methyl urocanate in ethanol at a concentration of 5×10^{-5} M. Spectra of the *trans* and *cis* isomers are shown in black and red, respectively, while the green spectra are associated with the final spectra of the irradiation experiments displayed in Figure 2(a) and (b) of the main text.

B. Photostability studies in dioxane, acetonitrile and buffer solutions

Figures S3-S5 show UV/vis absorption spectra of 5×10^{-5} M solutions of the indicated compounds using a 1 cm cuvette before and during at λ_{max} for the indicated irradiation time given in seconds. The inserts display the change of absorption at each λ_{max} (black dot curves) with the red percentage indicating the overall change in absorption.

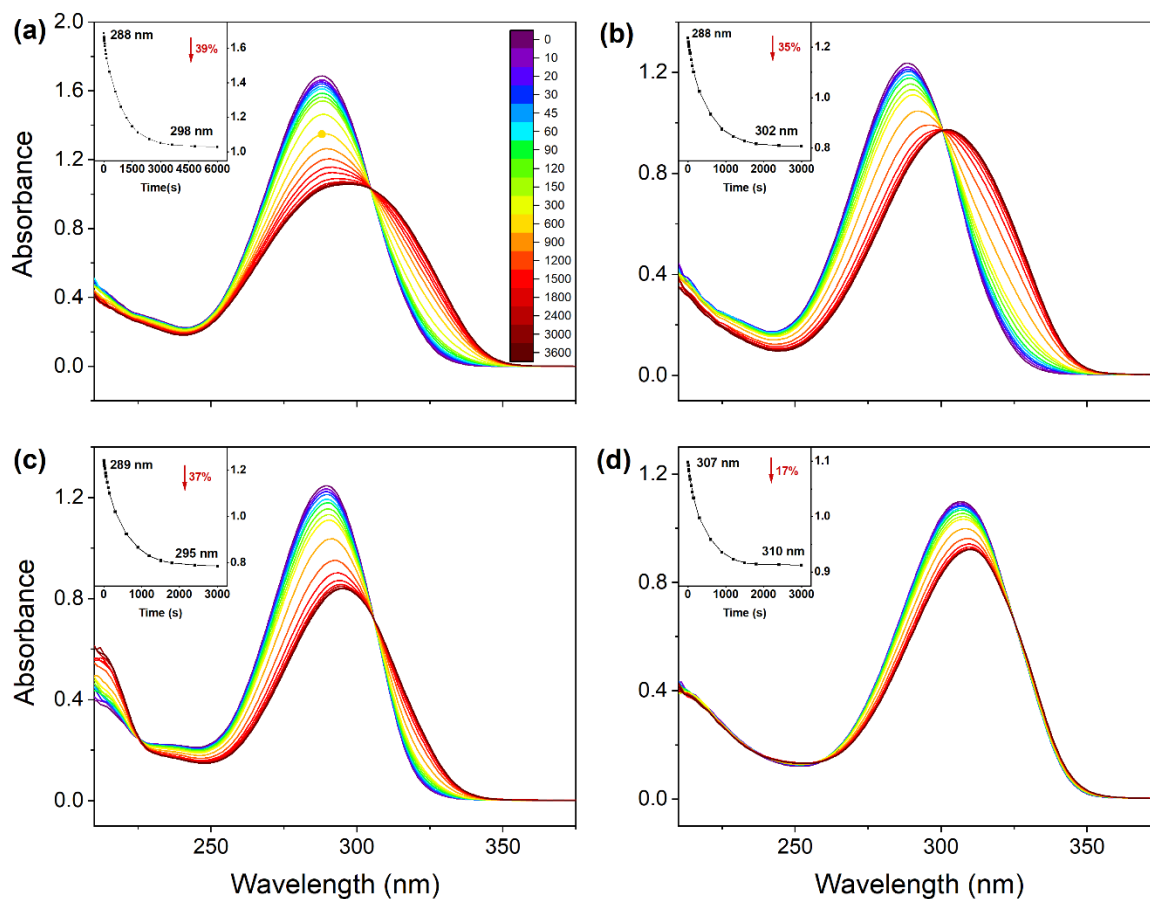


Figure S3. Long-term stability of (a) UA, (b) methyl urocanate, (c) N₃-methyl methyl urocanate, and (d) N₁-methyl methyl urocanate in dioxane before and during irradiation at λ_{max} for the indicated irradiation time given in seconds. Inserts display the change of absorption at each λ_{max} (black dot curves) with the red percentage indicating the overall change in absorption.

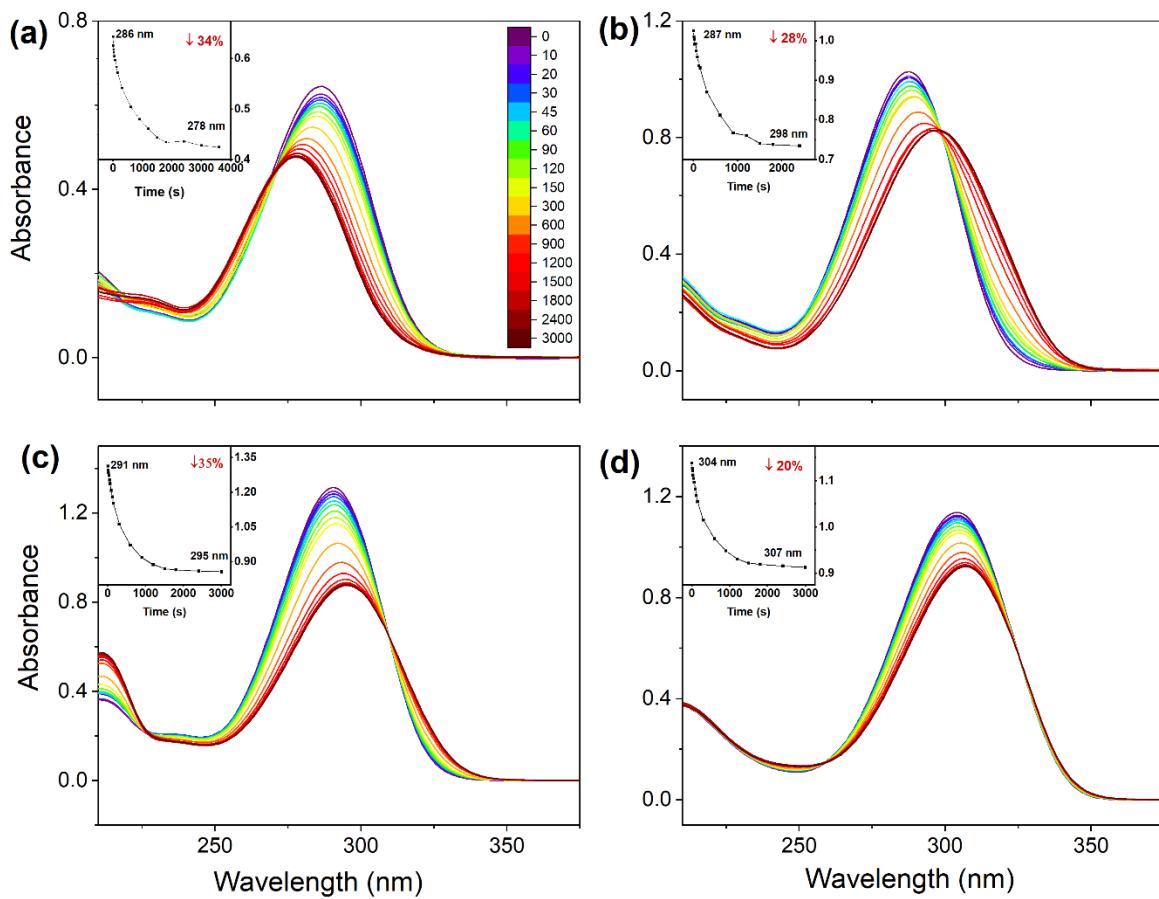


Figure S4. Long-term stability of (a) UA, (b) methyl urocanate, (c) N₃-methyl methyl urocanate, and (d) N₁-methyl methyl urocanate in acetonitrile before and during irradiation at λ_{\max} for the indicated irradiation time given in seconds. Inserts display the change of absorption at each λ_{\max} (black dot curves) with the red percentage indicating the overall change in absorption.

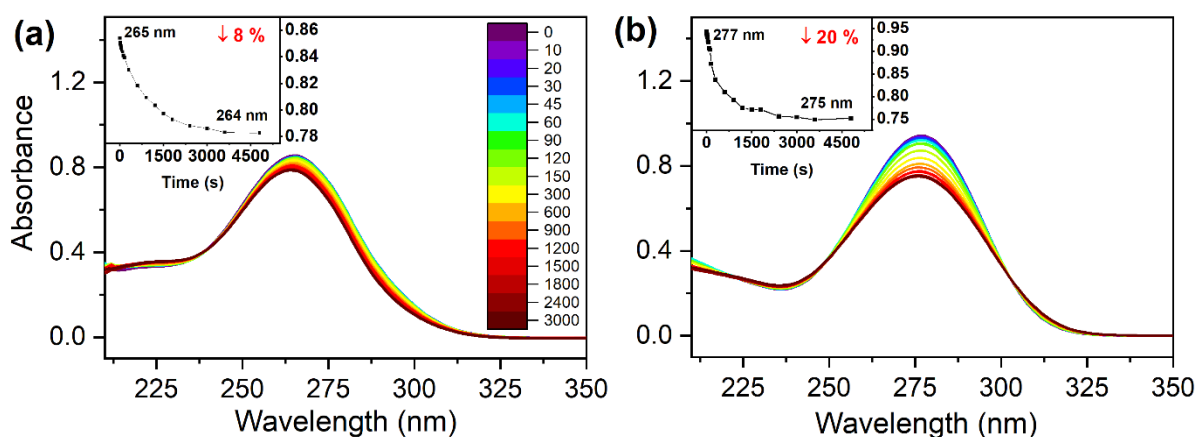


Figure S5. Long-term stability of UA in (a) pH 5.6 and (b) 7.2 buffer before and during irradiation at λ_{\max} for the indicated irradiation time given in seconds. Inserts display the change of absorption at each λ_{\max} (black dot curves) with the red percentage indicating the overall change in absorption.

3.2. NMR

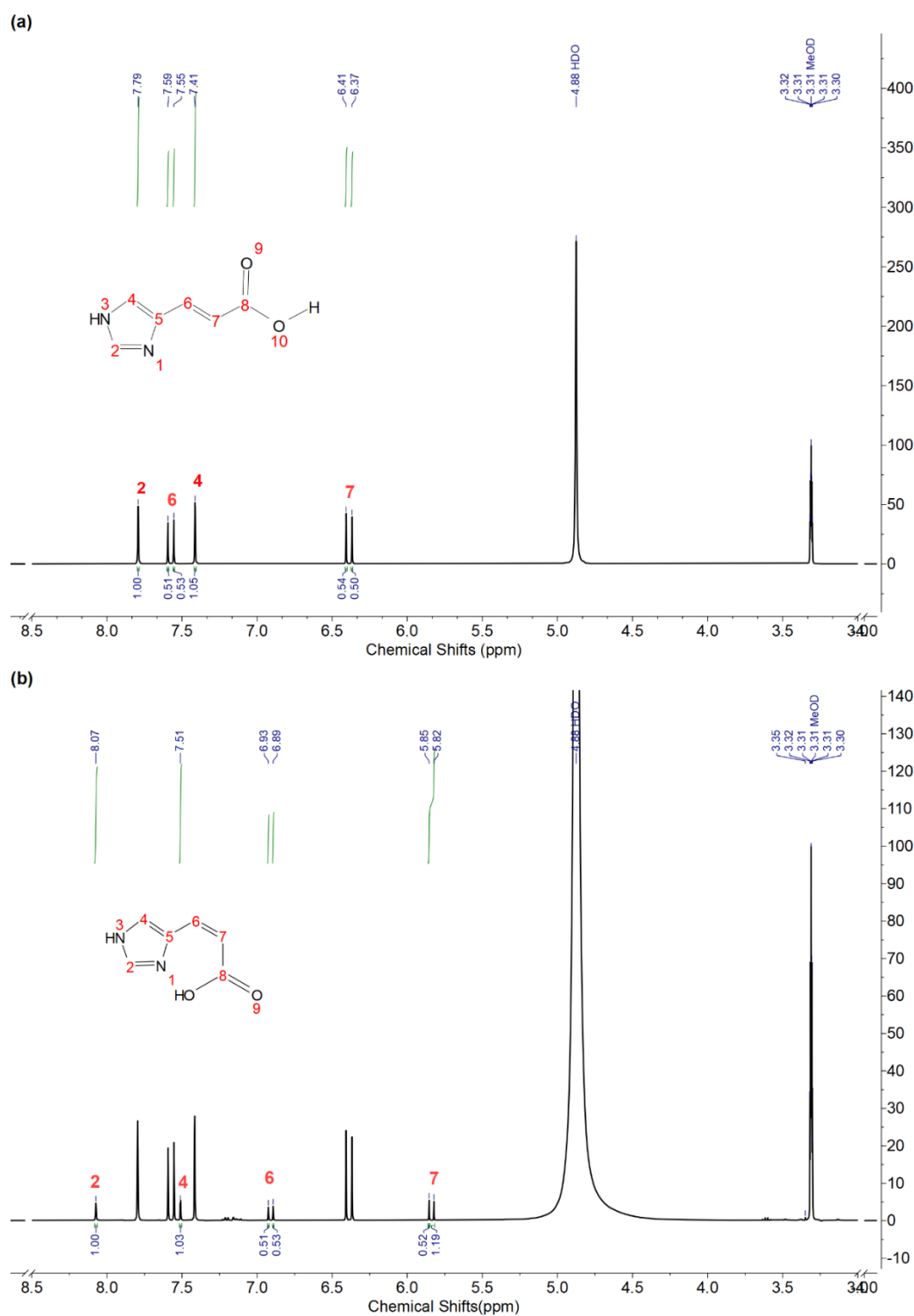


Figure S6. NMR spectrum of UA in MeOD before (a) and after (b) irradiation under conditions as indicated in Figure 2 of the main text.

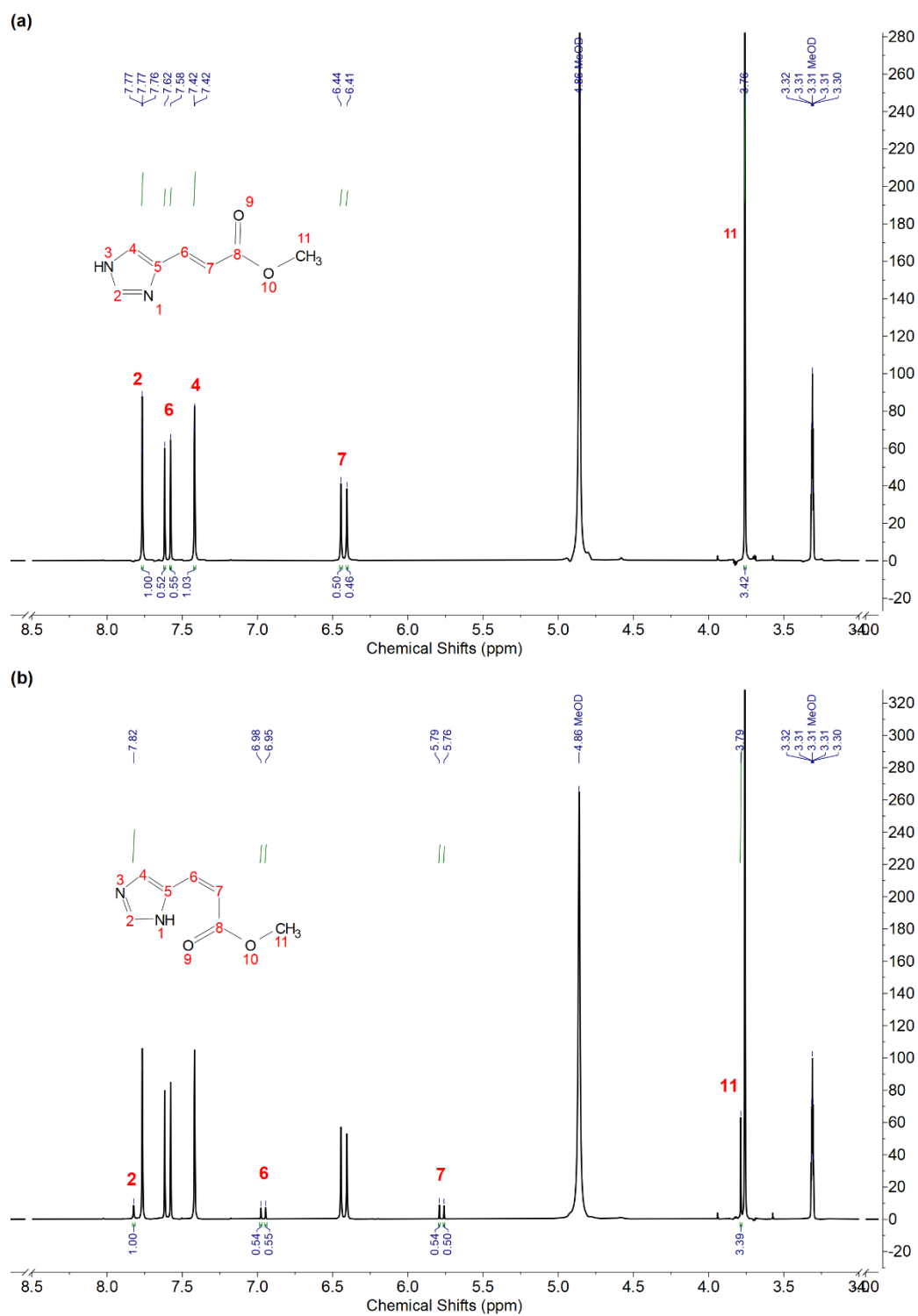


Figure S7. NMR spectrum of methyl urocanate in MeOD before (a) and after (b) irradiation under conditions as indicated in Figure 2 of the main text.

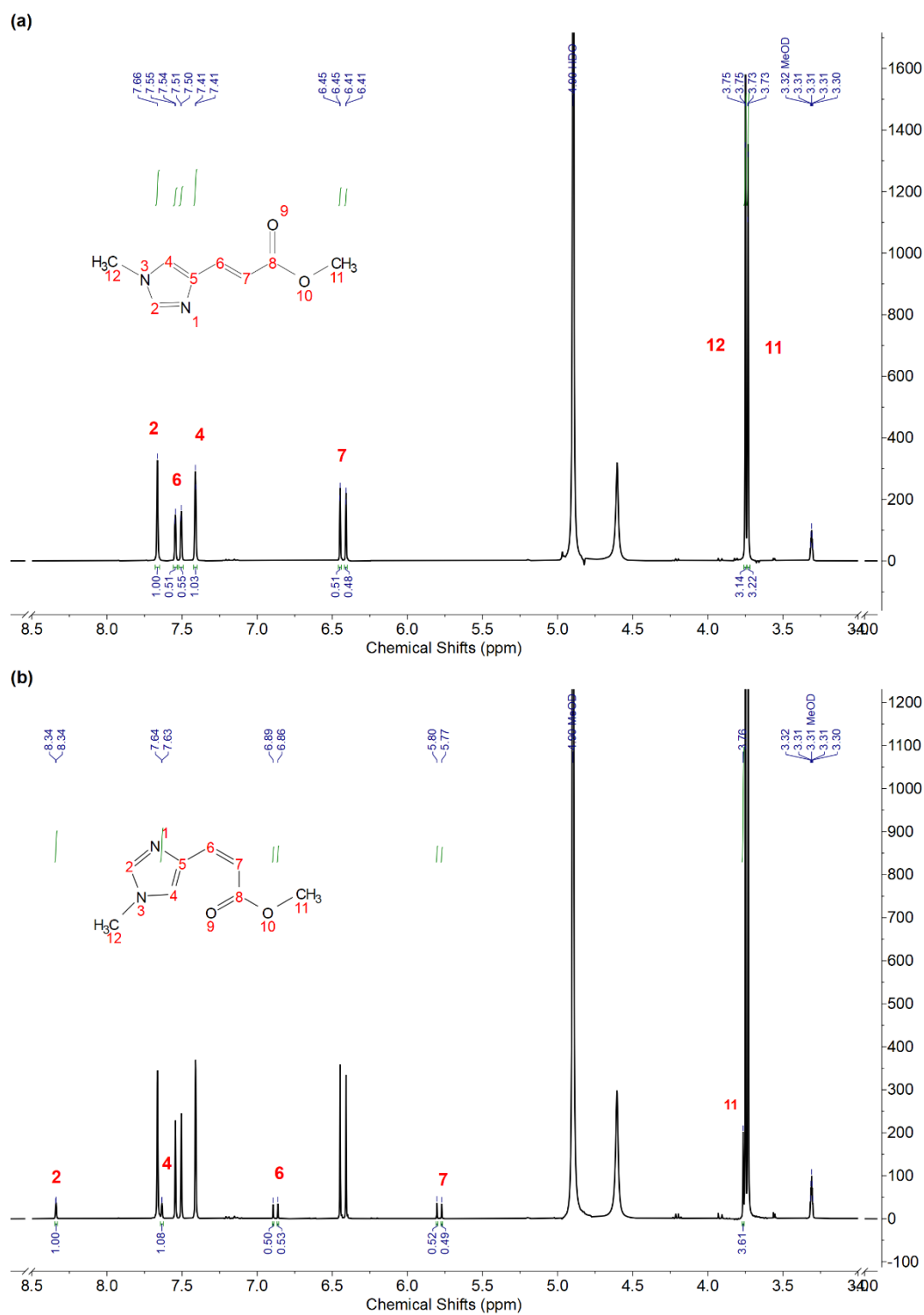


Figure S8. NMR spectrum of N_3 -methyl methyl urocanate in MeOD before (a) and after (b) irradiation under conditions as indicated in Figure 2 of the main text.

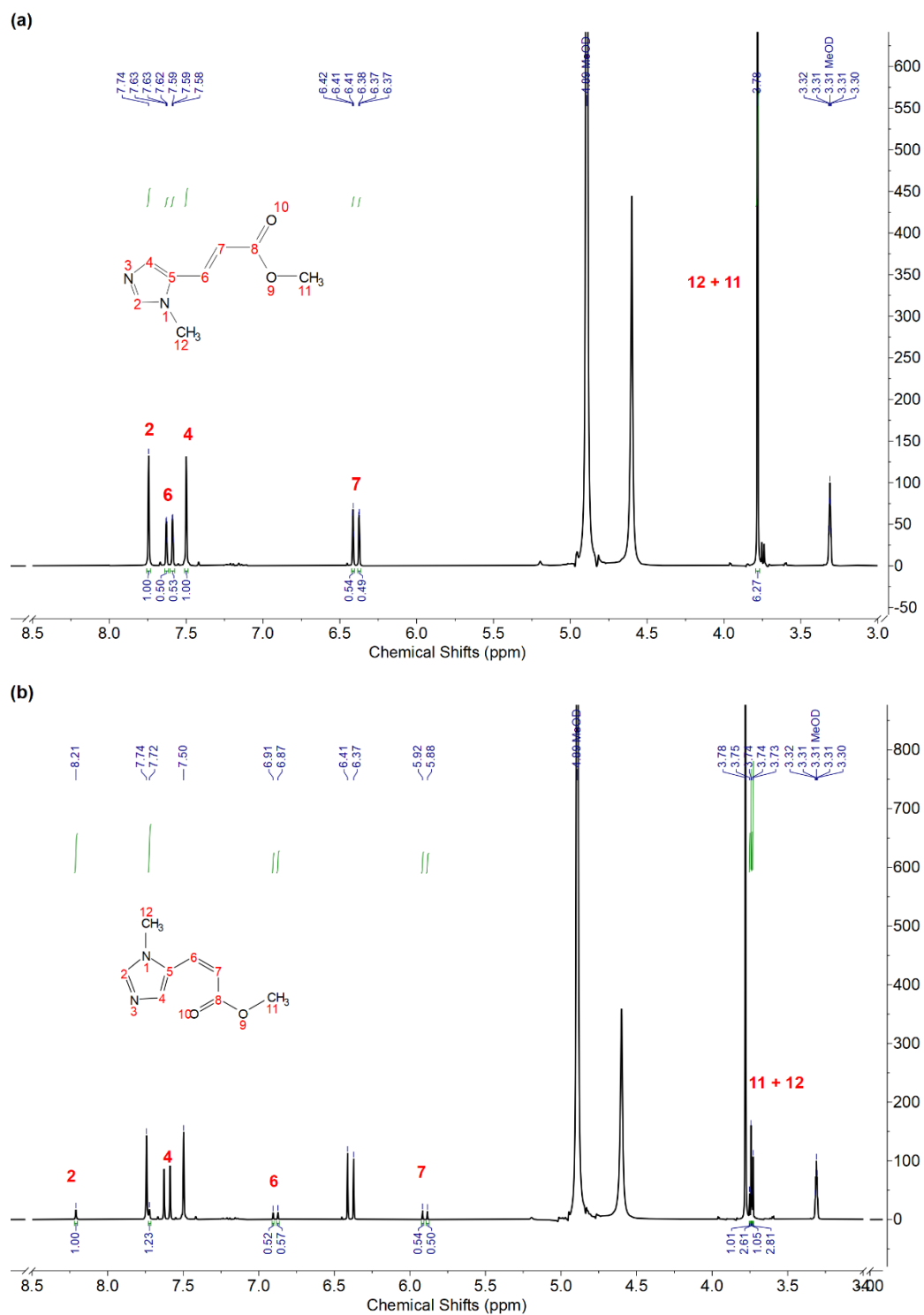


Figure S9. NMR spectrum of N_1 -methyl methyl urocanate in MeOD before (a) and after (b) irradiation under conditions as indicated in Figure 2 of the main text

3.3. FT-IR spectroscopy

A. Comparison UV/vis spectra irradiated samples in ethanol with spectra of isolated isomers

Figure S10 displays FT-IR spectra of the isolated *trans* and *cis* isomers of UA and methyl urocanate in ethanol as well as the spectrum recorded after prolonged irradiation (see the final spectrum in Figures 3(a) and (b)). These spectra confirm that the changes in the intensities of bands and the observation of new bands are due to the generation of the *cis* isomer. Figure 3(a) shows that *cis*-UA displays a much broader C=O stretch band than *trans*-UA. This is in line with the strong N \cdots H-O hydrogen bond in *cis*-UA (N₃H-TCT) and provides a consistent explanation for the broad band that appears in the 1660-1680 cm⁻¹ region upon UV irradiation.

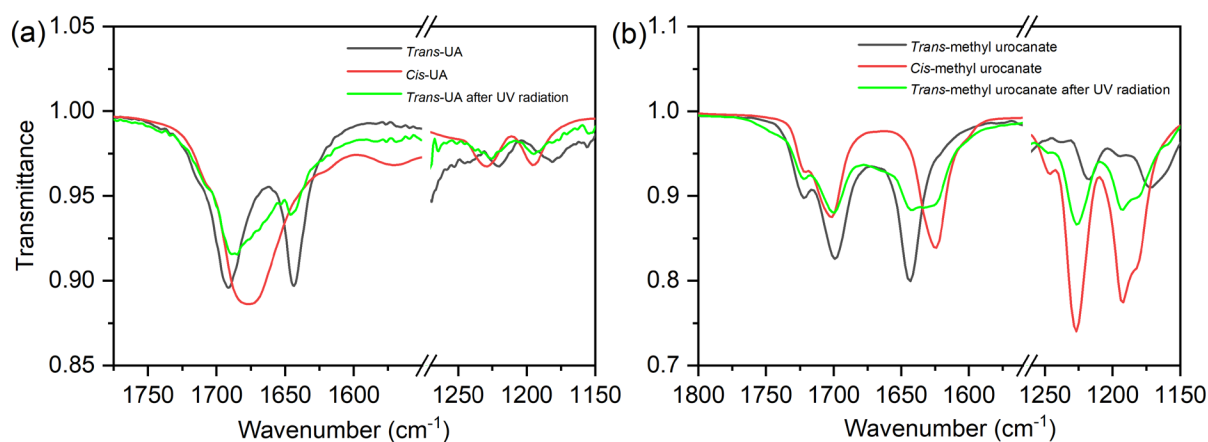


Figure S10. FT-IR spectra of 20 mM solutions of (a) UA and (b) methyl urocanate in ethanol. Spectra of the *trans* and *cis* isomers are shown in black and red, respectively, while the green spectra are associated with the final spectra of the irradiation experiments displayed in Figure 3(a) and (b) of the main text.

B. Photostability and conformational heterogeneity studies in ethanol, dioxane and acetonitrile

Figures S11-S13 display on the left side FT-IR spectra of 20 mM solutions of the indicated compounds using a BaF₂ cell with a spacer of 250 μm before and during irradiation at λ_{max} for the indicated irradiation time given in seconds (except in acetonitrile). The right side of the figures displays spectra simulated using DFT calculations at the B3LYP/6-31++G(d,p)/PCM level and scaling vibrational frequencies with a factor of 0.975. The blue (red) curves show simulated spectra using the ground-state energies of the *trans* (*cis*) isomers, which are given in Tables S1-S4, and a *trans* to *cis* ratio given in these Tables as well.

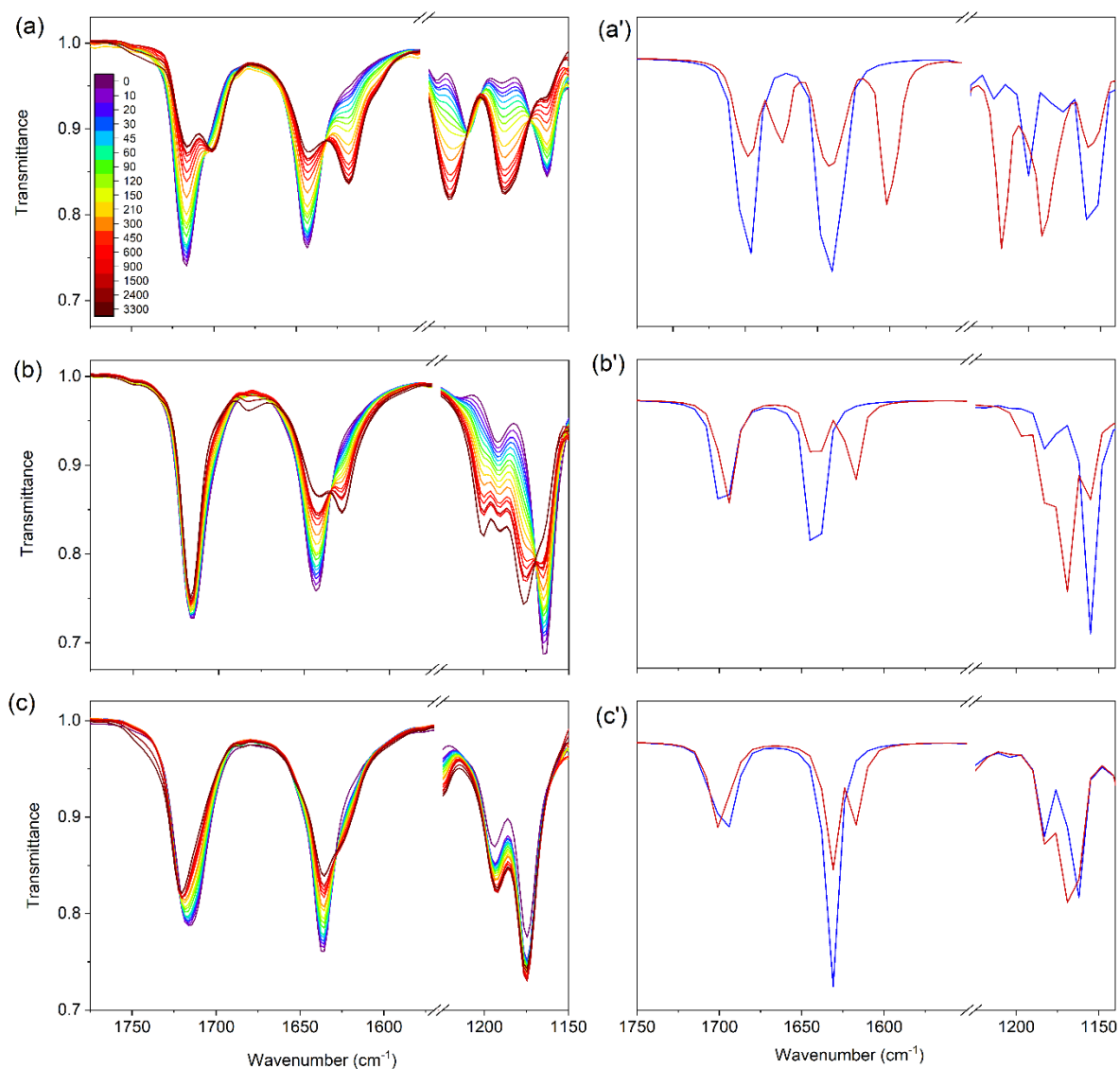


Figure S11. Long-term stability of methyl urocanate (a, a'), N₃-methyl methyl urocanate (b, b'), and N₁-methyl methyl urocanate (c, c') in dioxane at varying duration of irradiation at λ_{max} . Similar spectra could not be recorded for UA because of the limited solubility of UA in dioxane. Left panels display the experimentally recorded FT-IR spectra, the right panels simulated spectra before (blue) and after (red) irradiation (see section 3.3).

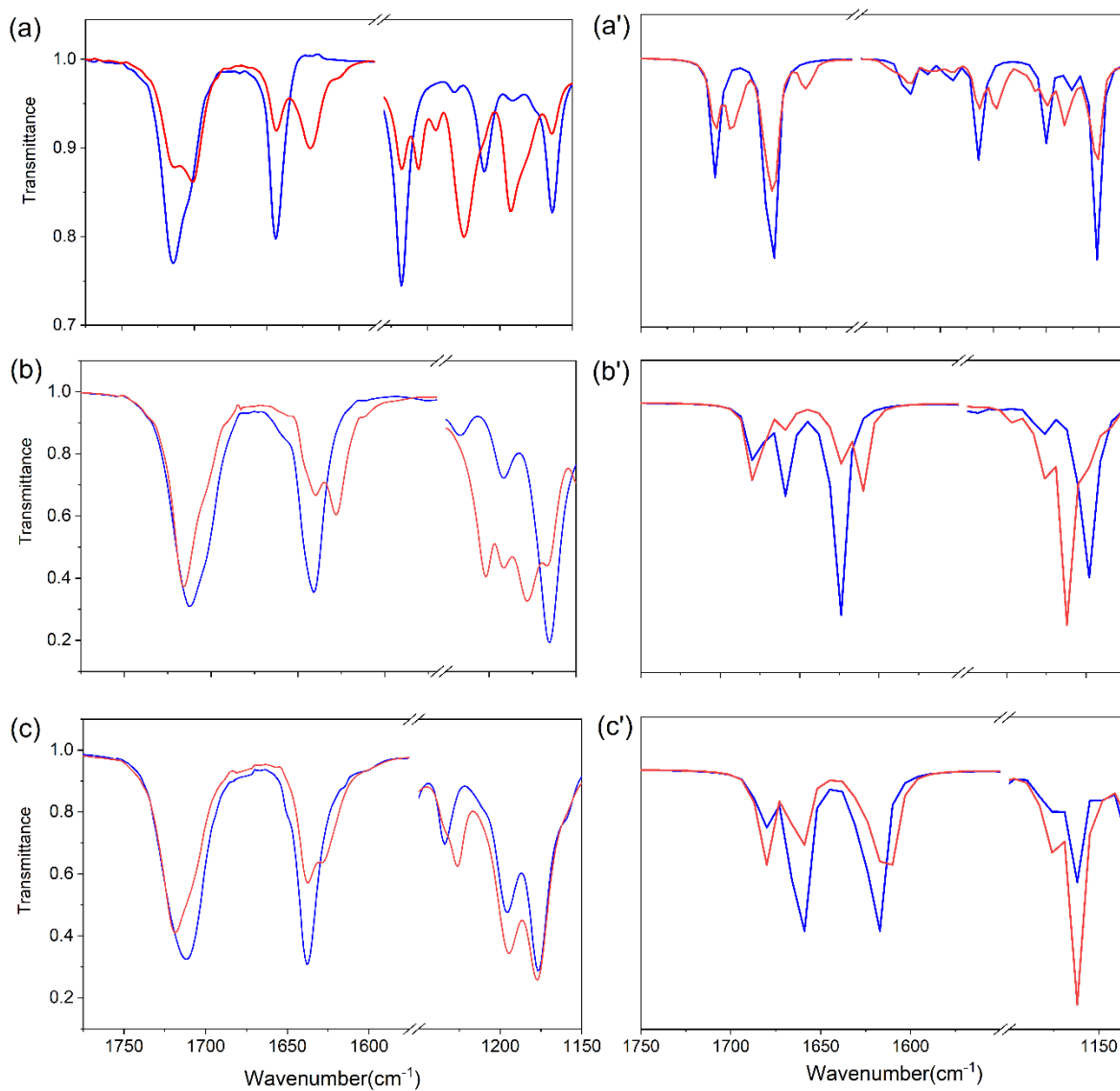


Figure S12. Long-term stability of methyl urocanate (a, a'), N₃-methyl methyl urocanate (b, b'), and N₁-methyl methyl urocanate (c, c') in acetonitrile before (blue) and after 15 minutes of UV radiation (red) at λ_{max} . Similar spectra could not be recorded for UA because of the limited solubility of UA in acetonitrile. Left panels display the experimentally recorded FT-IR spectra before (blue) and after 15 minutes of UV radiation (red), the right panels simulated spectra before (blue) and after (red) irradiation (see section 3.3).

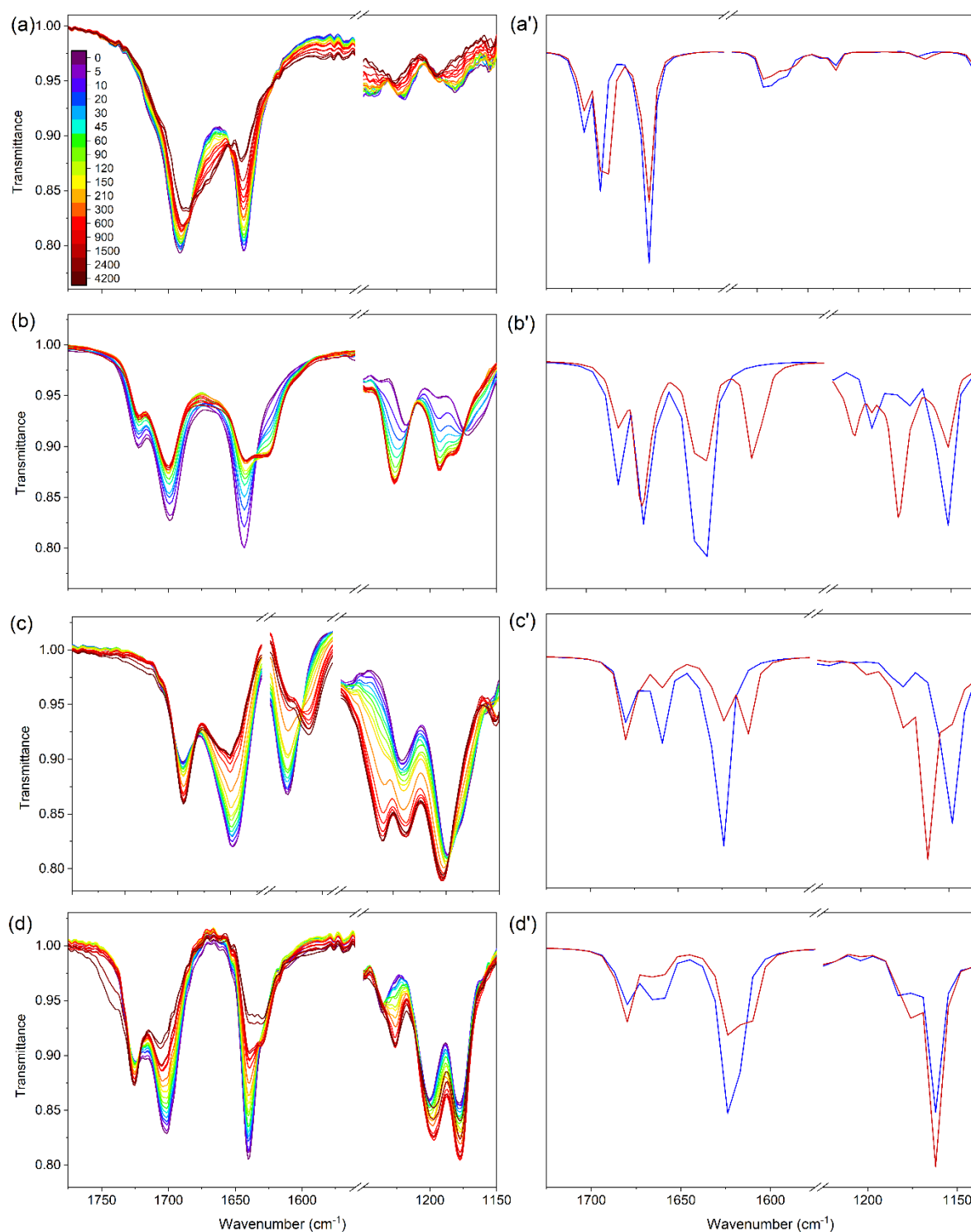


Figure S13. Long-term stability of UA (a, a'), methyl urocanate (b, b'), N₃-methyl methyl urocanate (c, c'), and N₁-methyl methyl urocanate (d, d') in ethanol at varying duration of irradiation at λ_{max} . Left panels display the experimentally recorded FT-IR spectra, the right panels simulated spectra before (blue) and after (red) irradiation (see section 3.3).

3.3. Population ratios used in FT-IR simulations

The ground state energy of each stable conformer has been obtained using DFT calculations at the B3LYP/6-31++G(d,p)/PCM level and is given in cm^{-1} with respect to the energy of the lowest-energy *trans* conformer. The (B/A) ratio gives the contribution of each conformer based on its ground state energy using the given *trans* to *cis* ratio that has been estimated by comparing experimental and simulated spectra. The B entries thus represent conformer distributions before irradiation, and A entries after irradiation. Dashes indicate that a particular conformation cannot be generated upon irradiation.

Table S1. Ground state energies of the most stable *trans* and *cis* conformers of urocanic acid.

Urocanic acid		Relative energies (cm^{-1})			
		Ethanol		Dioxane	Acetonitrile
		Energy	Ratio (B/A)	Energy	Energy
<i>Trans</i>	N ₃ H-TTC	0	0.56/0.39	0	0
	N ₃ H-TTT	126	0.30/0.21	215	121
	N ₁ H-TTC	386	0.09/0.06	215	392
	N ₁ H-TTT	522	0.05/0.04	389	528
<i>Cis</i>	N ₃ H-TCT	-638	0/0.30	172	-669
	N ₁ H-TCC	61	-	-774	94
	N ₃ H-TCC	2928	-	3424	2902

Table S2. Ground state energies of the most stable *trans* and *cis* conformers of methyl urocanate.

Methyl Urocanate		Relative energies (cm^{-1})					
		Ethanol		Dioxane		Acetonitrile	
		Energy	Ratio (B/A)	Energy	Ratio (B/A)	Energy	Ratio (B/A)
<i>Trans</i>	N ₃ H-TTC	0	0.61/0.30	0	0.59/0.30	0	0.61/0.27
	N ₃ H-TTT	221	0.21/0.10	333	0.12/0.06	214	0.22/0.10
	N ₁ H-TTC	350	0.11/0.06	207	0.22/0.10	355	0.11/0.05
	N ₃ H-CTC	459	0.07/0.04	-	-	455	0.07/0.03
	N ₁ H-TTT	-	-	432	0.07/0.04	-	-
<i>Cis</i>	N ₁ H-TCC	-17	0/0.50	-863	0/0.50	17	0/0.55
	N ₃ H-CCC	1284	-	836	-	1302	-
	N ₃ H-TCT	2907	-	3077	-	2896	-
	N ₃ H-TCC	2966	-	3227	-	2856	-

Table S3. Ground state energies of the most stable *trans* and *cis* conformers of N₃-methyl methyl urocanate.

N ₃ -methyl methyl urocanate		Relative energies (cm ⁻¹)					
		Ethanol		Dioxane		Acetonitrile	
		Energy	Ratio (B/A)	Energy	Ratio (B/A)	Energy	Ratio (B/A)
<i>Trans</i>	N ₃ H-TTC	0	0.67/0.20	0	0.76/0.27	0	0.66/0.17
	N ₃ H-TTT	235	0.21/0.06	344	0.14/0.05	229	0.23/0.07
	N ₃ H-CTC	433	0.08/0.02	505	0.07/0.02	429	0.09/0.02
	N ₃ H-CTT	639	0.03/0.01	653	0.03/0.01	640	0.03/0.01
<i>Cis</i>	N ₃ H-CCC	1267	0/0.7	819	0/0.65	1286	0/0.73
	N ₃ H-CCT	2940	-	1998	-	2033	-
	N ₃ H-TCC	2956	-	3468	-	2929	-
	N ₃ H-TCT	2940	-	3114	-	2929	-

Table S4. Ground state energies of the most stable *trans* and *cis* conformers of N₁-methyl methyl urocanate.

N ₁ -methyl methyl urocanate		Relative energies (cm ⁻¹)					
		Ethanol		Dioxane		Acetonitrile	
		Energy	Ratio (B/A)	Energy	Ratio (B/A)	Energy	Ratio (B/A)
<i>Trans</i>	N ₁ H-TTC	77	0.32/0.16	101	0.31/0.15	75	0.32/0.22
	N ₁ H-TTT	348	0.09/0.04	366	0.09/0.05	347	0.09/0.06
	N ₁ H-CTC	0	0.46/0.24	0	0.52/0.26	0	0.46/0.32
	N ₁ H-CTT	259	0.13/0.06	396	0.08/0.04	252	0.14/0.10
<i>Cis</i>	N ₁ H-CCC	1192	0/0.50	819	0/0.50	1187	0/0.3
	N ₁ H-CCT	1891	-	1998	-	1884	-
	N ₁ H-TCC	2681	-	3468	-	2086	-
	N ₁ H-TCT	3120	-	3114	-	3116	-

4. Femtosecond transient absorption spectra in acetonitrile

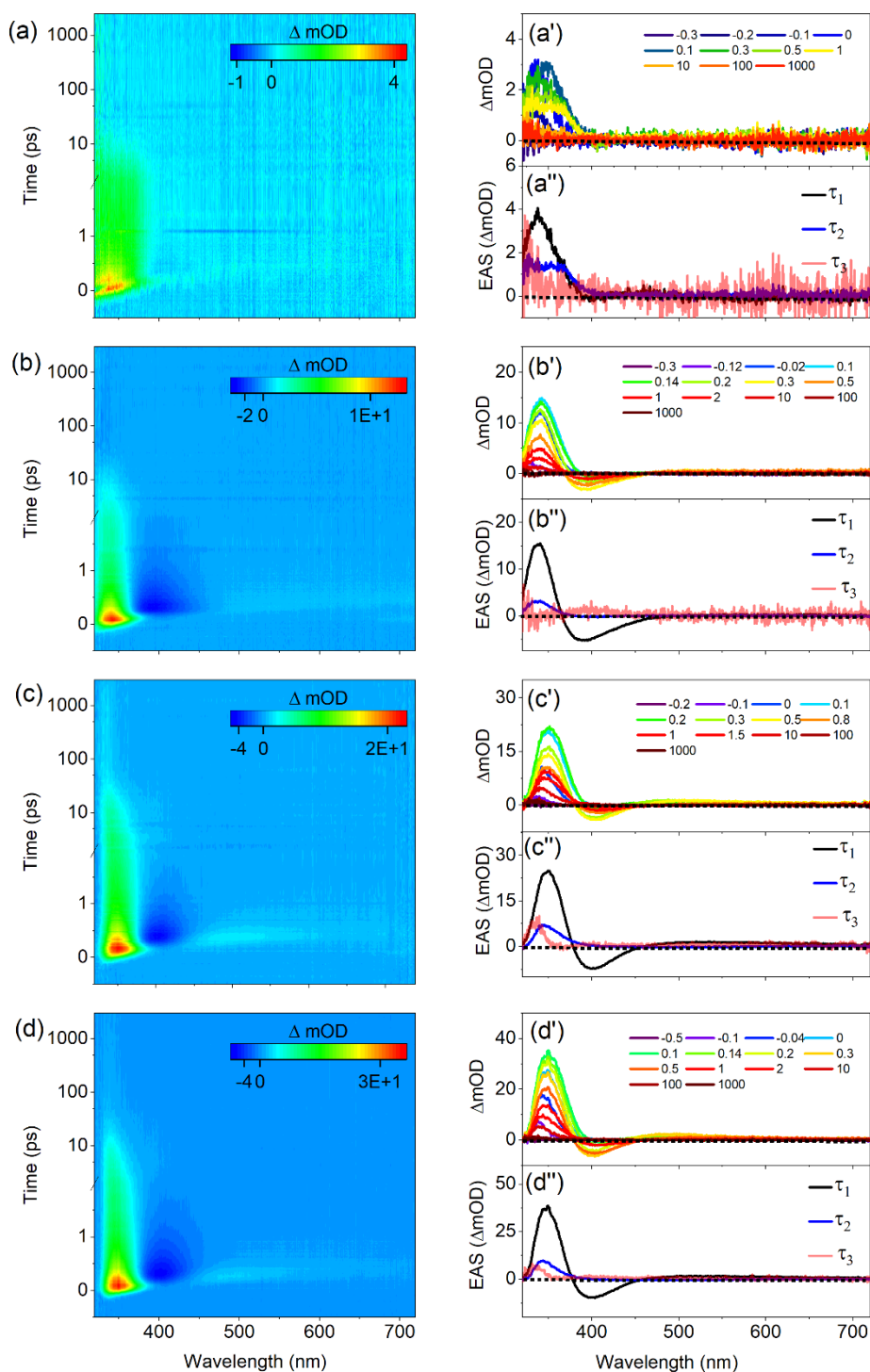


Figure S14. Transient absorption spectra displayed as false color heat maps of (a) UA, (b) methyl urocanate, (c) N₃-methyl methyl urocanate and (d) N₁-methyl methyl urocanate in acetonitrile excited at 287, 287, 287, and 300 nm, respectively, with time delay plotted linearly until 2 ps and then as a logarithmic scale from 2 ps to 2500 ps. Panels (a')-(d') display lineouts at selected pump-probe delays, while panels (a'')-(d'') show the EADS resulting from a global analysis of the data with EADS3 multiplied by 5 for visual aid.

5. Calculations of vertical and adiabatic excitation energies

Tables S5-S8 report vertical excited state energies that have been obtained using TD-DFT calculations at the wB97XD/cc-pVDZ/PCM level at the wB97XD/cc pVDZ/PCM optimized ground state geometry. Adiabatic energies have been obtained from optimizations of the geometry of the pertaining state.

Table S5. Vertical and adiabatic excitation energies (eV) of the lower electronically excited singlet states of urocanic acid (N₃H-TTC) with oscillator strengths given in parentheses.

		Singlet excited states	
		Vertical	Adiabatic
Dioxane	S ₁ ($\pi\pi^*$)	4.79 (0.67)	4.43 (0.77)
	S ₂ ($n\pi^*$)	5.05 (0.01)	4.40 (0) ^(a)
Acetonitrile	S ₁ ($\pi\pi^*$)	4.49 (0.87)	4.11 (0.89)
	S ₂ ($n\pi^*$)	5.10 (0)	4.51(0) ^(b)
Ethanol	S ₁ ($\pi\pi^*$)	4.51 (0.86)	4.12 (0.89)
	S ₂ ($n\pi^*$)	5.10 (0)	4.51 (0) ^(b)
pH 5.6 (H⁺UA⁻)	S ₁ ($n\pi^*$)	4.01 (0)	3.03 (0)
	S ₂ ($n\pi^*$)	4.14 (0)	^(c)
	S ₃ ($\pi\pi^*$)	4.91 (0.18)	4.29 (0.10) ^(d)
	S ₄ ($\pi\pi^*$)	5.02 (0.65)	^(c)
pH 7.2 (UA⁻)	S ₁ ($n\pi^*$)	4.43 (0)	3.46 (0)
	S ₂ ($n\pi^*$)	4.61 (0)	4.39 (0)
	S ₃ ($\pi\pi^*$)	5.02 (0.84)	4.51 (0.81) ^(e)
	S ₄ ($\pi\pi^*$)	5.53 (0.09)	4.98 (0.20)

^(a) Excitation energy obtained for geometry optimization under C_s symmetry restrictions. In dioxane an imaginary frequency of 57.4 cm⁻¹ for a O₉=C₈-OH torsional mode is found. Optimization under non-planar geometry conditions lowers the energy by less than 1 cm⁻¹, implying that effectively C_s symmetry is retained.

^(b) Excitation energy obtained for geometry optimization under C_s symmetry restrictions. In acetonitrile an imaginary frequency of 340.1 cm⁻¹ for a C₆=C₇-H bending mode, and in ethanol an imaginary frequency of 260.6 cm⁻¹ for a C₆=C₇-H bending mode. Optimization under non-planar geometry conditions leads in both cases to root switching with S₁.

^(c) Geometry optimization under C_s symmetry restrictions leads in pH 5.6 calculations to root switching of S₂ and S₄ with S₁ and S₃, respectively, while in pH 7.2 calculations root switching of S₂ with S₁ occurs.

^(d) Excitation energy obtained for geometry optimization under C_s symmetry restrictions. At optimized geometry an imaginary frequency of 209.2 cm⁻¹ for a C₇-C₈-O₁₀-H torsional mode is found, optimization under non-planar geometry conditions leads to root switching with S₁.

^(e) Excitation energy obtained for geometry optimization under C_s symmetry restrictions. At optimized geometry an imaginary frequency of 398.8 cm⁻¹ for a H-C₆=C₇-H torsional mode is obtained, optimization under non-planar geometry conditions leads to root switching with S₂.

Table S6. Vertical and adiabatic excitation energies (eV) of the lower electronically excited singlet states of methyl urocanate (N₃H-TTC) with oscillator strengths given in parentheses.

Solvent		Singlet excited states	
		Vertical	Adiabatic
Dioxane	S ₁ ($\pi\pi^*$)	4.79 (0.83)	4.23 (0.84)
	S ₂ ($n\pi^*$)	5.06 (0)	4.44 (0)
Acetonitrile	S ₁ ($\pi\pi^*$)	4.50 (0.93)	4.11 (0.96)
	S ₂ ($n\pi^*$)	5.12 (0)	4.55 (0) ^(a)
Ethanol	S ₁ ($\pi\pi^*$)	4.51 (0.93)	4.12 (0.95)
	S ₂ ($n\pi^*$)	5.12 (0)	4.55 (0) ^(a)

^(a) Excitation energy obtained for geometry optimization under C_s symmetry restrictions. In acetonitrile, an imaginary frequency of 651.5 cm⁻¹ for an H-C₆=C₇-H out-of-plane twisting mode is found, while in ethanol an imaginary frequency of 469.5 cm⁻¹ for an H-C₆=C₇-H out-of-plane twisting mode is obtained. In both solvents optimization under non-planar geometry conditions leads to root switching with S₁.

Table S7. Vertical and adiabatic excitation energies (eV) of the lower electronically excited singlet states of N₃-methyl methyl urocanate (N₃H-TTC) with oscillator strengths given in parentheses.

Solvent		Singlet excited states	
		Vertical	Adiabatic
Dioxane	S ₁ ($\pi\pi^*$)	4.79 (0.90)	4.35 (0.92)
	S ₂ ($n\pi^*$)	5.06 (0)	4.45 (0) ^(a)
Acetonitrile	S ₁ ($\pi\pi^*$)	4.44 (0.99)	4.05 (1.03)
	S ₂ ($n\pi^*$)	5.13 (0)	4.55 (0)
Ethanol	S ₁ ($\pi\pi^*$)	4.45 (1.00)	4.06 (1.02)
	S ₂ ($n\pi^*$)	5.12 (0)	4.55 (0) ^(a)

^(a) Excitation energy obtained for geometry optimization under C_s symmetry restrictions. In dioxane an imaginary frequency of 38.1 cm⁻¹ for a C₁₀-OCH₃ out-of-plane twisting mode is found, while in ethanol an imaginary frequency of 2386.1 cm⁻¹ for an H-C₆=C₇-H out-of-plane twisting mode is obtained. In both solvents, the optimization under non-planar geometry conditions leads to root switching with S₁.

Table S8. Vertical and adiabatic excitation energies (eV) of the lower electronically excited singlet states of N₁-methyl methyl urocanate (N₁H-CTC and N₁H-TTC) with oscillator strengths given in parentheses.

	Solvent		Singlet excited states	
			Vertical	Adiabatic
N ₁ H-CTC	Dioxane	S ₁ ($\pi\pi^*$)	4.29 (0.73)	3.97 (0.70)
		S ₂ ($n\pi^*$)	5.00 (0)	4.38 (0) ^(a)
	Acetonitrile	S ₁ ($\pi\pi^*$)	4.11 (0.82)	3.74 (0.81)
		S ₂ ($n\pi^*$)	5.05 (0)	4.48 (0)
	Ethanol	S ₁ ($\pi\pi^*$)	4.11 (0.82)	3.75 (0.8)
		S ₂ ($n\pi^*$)	5.05 (0)	4.44 (0)
N ₁ H-TTC	Dioxane	S ₁ ($\pi\pi^*$)	4.49 (0.84)	4.19 (0.87)
		S ₂ ($n\pi^*$)	5.05 (0)	4.44 (0)
	Acetonitrile	S ₁ ($\pi\pi^*$)	4.28 (0.97)	3.94 (0.99)
		S ₂ ($n\pi^*$)	5.10 (0)	4.54 (0)
	Ethanol	S ₁ ($\pi\pi^*$)	4.29 (0.96)	3.95 (0.99)
		S ₂ ($n\pi^*$)	5.10 (0)	4.54 (0)

^(a) Excitation energy obtained for geometry optimization under C_s symmetry restrictions. In dioxane an imaginary frequency of 211.2 cm⁻¹ for an H-C₆=C₇-H out-of-plane twisting mode is found, and optimization under non-planar geometry conditions leads to root switching with S₁.

6. Electron scavenging studies

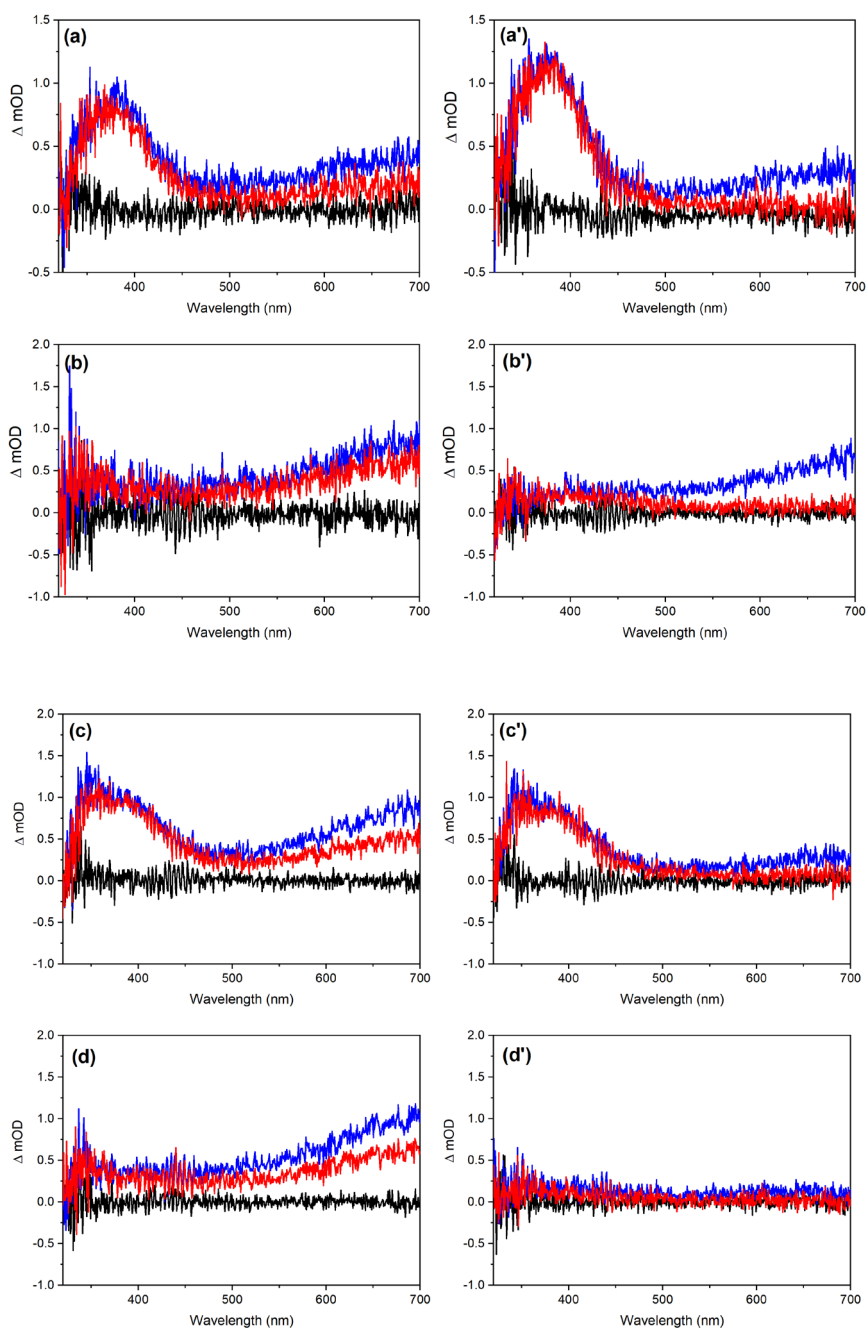


Figure S15. Transient absorption spectra obtained at -0.5 (black), 100 (blue), and 1000 (red) ps for UA in pH 5.6 (H^+UA^-) ((a) and (b)) and 7.2 (UA^-) ((c) and (d)) buffer solutions. (a')-(d') indicate their spectral changes after adding 0.2 M KNO_3 solution. In (a/a') and (c/c') excitation occurs at 266 nm, while in (b/b') and (d/d') an excitation wavelength of 306 nm is employed.

7. Nanosecond transient absorption spectra in buffer solutions

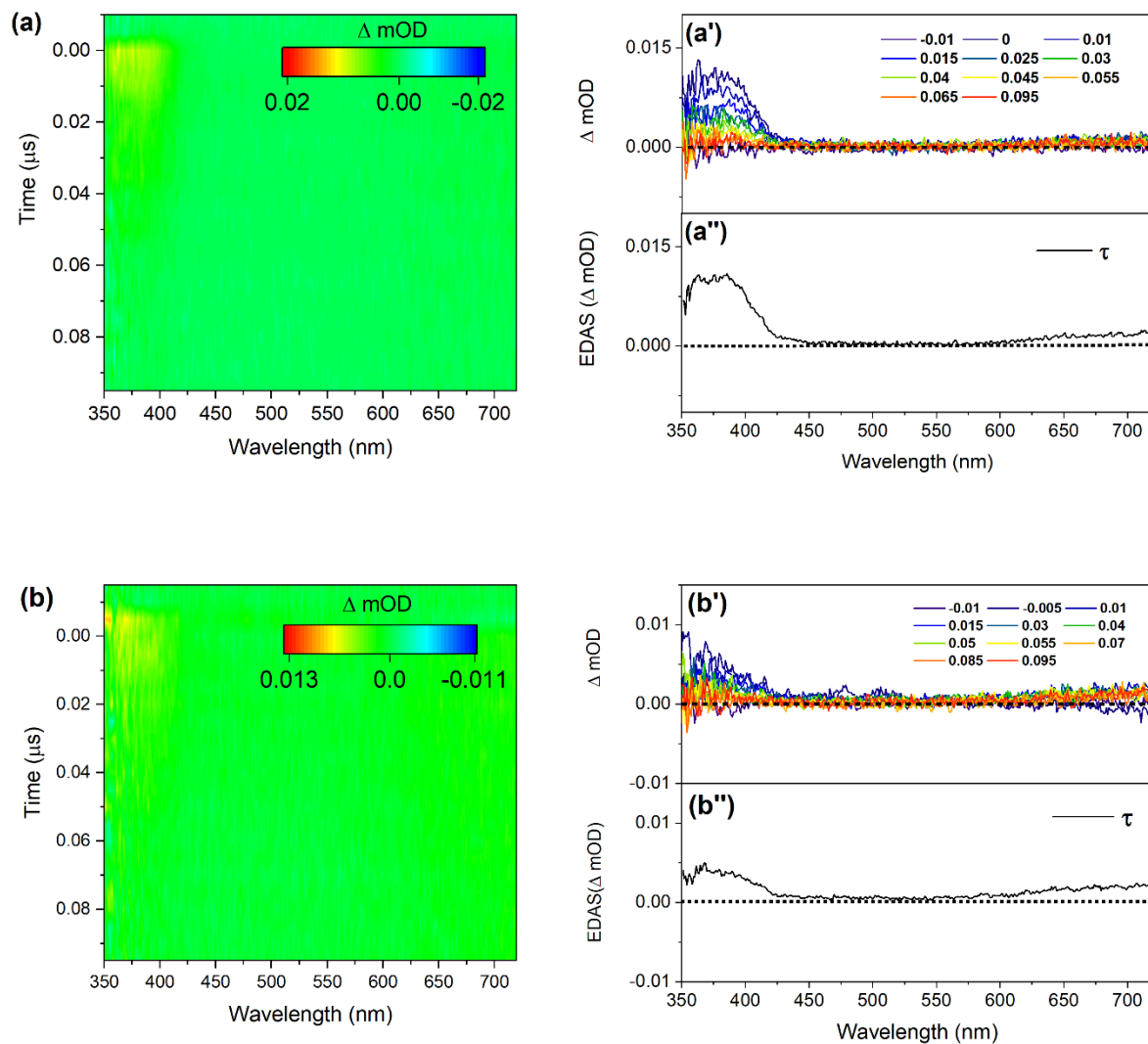


Figure S16. Nanosecond transient absorption spectra displayed as false color heat maps of UA in pH 5.6 (H^+UA^-) (a) and pH 7.2 (UA^-) (b) buffer solutions excited at 266 nm, respectively. Panels (a') and (b') display lineouts at selected pump-probe delays, while panels (a'') and (b'') show the EADS resulting from a global analysis of the data.

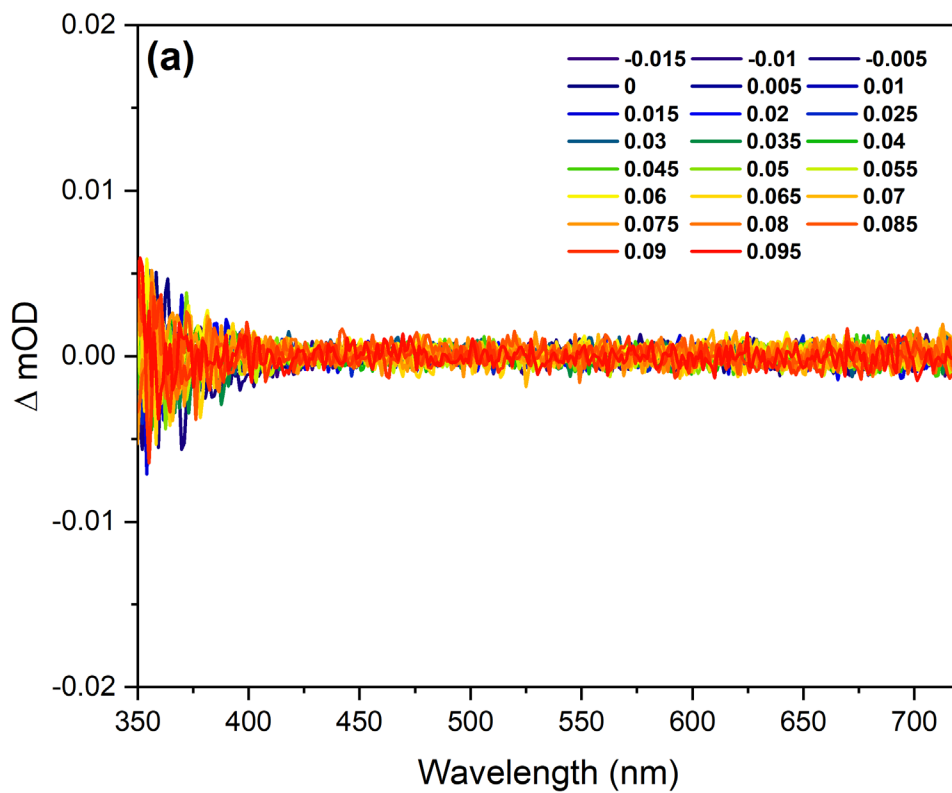


Figure S17. Nanosecond transient absorption spectra of UA in pH 5.6 (H^+UA^-) (left) and pH 7.2 (UA^-) (right) buffer solutions excited at 306 nm.

8. Supplemental references

- [1] J. Fan, A.K. Lemmens, H. Sanders, M. Hilbers, W. Roeterdink, W.J. Buma. **2024**, DOI: 10.1039/d4cp02087a.
- [2] Quest Calculate™ Acetate Buffer (pH=3.6 to 5.6) Preparation and Recipe. AAT Bioquest, Inc., 2022.
- [3] Quest Calculate™ Phosphate Buffer (pH=5.8 to 7.4) Preparation and Recipe. AAT Bioquest, Inc., 2022.
- [4] C. Ruckebusch, M. Sliwa, P. Pernot, A. De Juan, R. Tauler. *J. Photochem. Photobiol. C: Photochem.* **2012**, *13*, 1-27.
- [5] L.A. Baker, V.G. Stavros. *Sci. Prog.* **2016**, *99*, 282-311.
- [6] M.W.H. Hoorens, M. Medved', A.D. Laurent, M. Di Donato, S. Fanetti, L. Slappendel, M.F. Hilbers, B.L. Feringa, W.J. Buma, W. Szymański. *Nat. Commun.* **2019**, *10*, 2390.
- [7] J.J. Snellenburg, S. Laptinok, R. Seger, K.M. Mullen, I.H.M. van Stokkum. *J. Stat. Softw.* **2012**, *49*, 1-22.
- [8] J.D. Chai, M. Head-Gordon. *Phys. Chem. Chem. Phys.* **2008**, *10*, 6615-6620.
- [9] J. Tomasi, B. Mennucci, R. Cammi, *Chem. Rev.* **2005**, *105*, 2999-3094.
- [10] A.D. Becke. *J. Chem. Phys.* **1993**, *98*, 5648-52.
- [11] M.D. Halls, H.B. Schlegel. *J. Chem. Phys.* **1998**, *109*, 10587-10593.
- [12] J.K. Martens, J. Grzetic, G. Berden, J. Oomens. *Nat. Commun.* **2016**, *7*, 11754.
- [13] J.K. Martens, J. Grzetic, G. Berden, J. Oomens. *Int. J. Mass. Spectrom.* **2015**, *377*, 179-187.
- [14] M.J. Frisch *et al.*. Gaussian16. Revision C. 01. Gaussian Inc., Wallingford, CT, USA, **2016**.